

Article

Outer Topology Network Synchronization Using Chaotic Nodes with Hidden Attractors

Carlos Andrés Villalobos-Aranda ¹, Adrian Arellano-Delgado ^{2,3}, Ernesto Zambrano-Serrano ⁴,
Javier Pliego-Jiménez ^{1,2} and César Cruz-Hernández ^{1,*}

- ¹ Electronics and Telecommunication Department, Scientific Research and Advanced Studies Center of Ensenada, Ensenada 22860, Mexico; cvillalobos@cicese.edu.mx (C.A.V.-A.); jpliego@cicese.mx (J.P.-J.)
² National Council of Science and Technology, Ciudad de Mexico 03940, Mexico; adrian.arellano@uabc.edu.mx
³ Engineering, Architecture and Design Faculty, Autonomous University of Baja California, Ensenada 22860, Mexico
⁴ Facultad de Ingeniería Mecánica y Eléctrica, Universidad Autónoma de Nuevo León, San Nicolás de los Garza 66455, Mexico; ernesto.zambranos@uanl.edu.mx
* Correspondence: ccruz@cicese.mx; Tel.: +52-(646)175-05-00 (ext. 25300)

Abstract: This paper addresses the synchronization problem in outer topology networks using chaotic nodes with hidden attractors. Specifically, we analyze bidirectionally coupled networks with various inner–outer coupling topologies to identify the optimal configuration that encourages outer synchronization. The inner–outer coupled networks incorporate a chaotic system capable of generating hidden attractors. To assess the stability of the synchronization state, we conduct numerical simulations and examine the maximum Lyapunov exponent of the generic variational equations. Our results reveal the most suitable bidirectional inner–outer coupling network topology for achieving outer synchronization.

Keywords: outer synchronization; inner–outer topology; master stability function; chaos; hidden attractors

MSC: 93C10; 65F45; 15A24; 65K10



Citation: Villalobos-Aranda, C.A.; Arellano-Delgado, A.; Zambrano-Serrano, E.; Pliego-Jiménez, J.; Cruz-Hernández, C. Outer Topology Network Synchronization Using Chaotic Nodes with Hidden Attractors. *Axioms* **2023**, *12*, 634. <https://doi.org/10.3390/axioms12070634>

Academic Editors: Yang (Felix) Lou, Guanrong (Ron) Chen and Lin Wang

Received: 30 April 2023
Revised: 20 June 2023
Accepted: 25 June 2023
Published: 27 June 2023



Copyright: © 2023 by the authors. Licensee MDPI, Basel, Switzerland. This article is an open access article distributed under the terms and conditions of the Creative Commons Attribution (CC BY) license (<https://creativecommons.org/licenses/by/4.0/>).

1. Introduction

A phenomenon observed in nature, particularly in animals, is the emergent collective behavior of synchronization, i.e., the temporal adjustment of events between two or more objects or subjects, see [1]. An example of this can be seen in [2], where an analysis of emergent synchronization in ecological systems is presented. Another similar paradigm is seen in [3–6], where the authors analyze collective behaviors, particularly in small-world networks.

In the last few years, the study of collective emergent behaviors in nature has gained significant attention from the scientific community. Synchronization phenomena are interesting collective behaviors found in multiple scientific areas, such as mathematics, computer science, physics, chemistry, etc., see [7–12].

Now, in addition to studies related to this behavior observed in nature, recent research has focused on analyzing networks with chaotic systems in order to prove that synchronization is possible. For example, in [13], the authors presented a synchronization scheme by using a control law obtained from some definitions of graph theory.

It is worth noting that there are two methods used to attain synchronization: unidirectional coupling and bidirectional coupling, as stated in [14]. Bidirectional coupling is the synchronization type used for each network presented in this work. It is remarkable that in recent works, some researchers have studied the outer synchronization of networks, such as in [15], where the outer synchronization of networks using an impulse type control was presented.

Moreover, in [16], the authors presented an adaptive outer synchronization of networks for the identification of unknown parameters between two time-delayed coupled networks. Given the recent works related to outer synchronization, it can be seen that the analysis of the outer coupling topology of networks is an interesting problem to address.

Hidden attractors in chaotic systems have received significant attention in the field of complex systems and network dynamics due to their distinctive characteristics. These systems are characterized by the absence of a homoclinic or heteroclinic orbit, making the verification of chaos through the Shilnikov method unsuitable. Such attractors can be found in systems without equilibrium points or in systems with only one stable equilibrium point. Specifically, the basin of attraction of a hidden attractor does not intersect with any unstable equilibrium point. The most notable difference between hidden attractors and self-excited attractors lies in the respective basin of attraction. The basin of attraction of a hidden attractor does not intersect with any small neighborhood surrounding an equilibrium point, whereas the basin of attraction of a self-excited attractor intersects with certain unstable equilibrium points [17]. Consequently, hidden attractors and self-excited attractors exhibit entirely distinct dynamic characteristics.

Considering the aforementioned gaps in the literature, this paper aims to provide a comprehensive analysis and comparison of various inner–outer coupling topologies in networks, in order to identify the optimal configuration for achieving inner–outer synchronization.

This work is organized as follows. In Section 2, we provide brief preliminaries regarding inner–outer coupling schemes and the synchronization of complex networks. In Section 3, we present the master stability function approach, which is the analysis method used to study and compare the synchronization state stability of the different inner–outer coupling topologies. In Section 4, we described an interesting chaotic system that has hidden attractors and a coexistence property. In Section 5, we present different scenarios where the inner–outer coupling network topologies are analyzed. Finally, the conclusions are drawn in Section 6.

2. Complex Dynamical Networks

In this section, we provide brief preliminaries regarding inner–outer coupling schemes and present the synchronization of complex networks. In a simple way, we consider a set of M networks, each one composed of N nodes. The inner coupling topology (i.e., coupling of the nodes in a network) is represented by an inner coupling matrix $\mathbf{A}_{\text{inner}}$; on the other hand, the outer coupling topology (i.e., the coupling among networks) is represented by an outer coupling matrix $\mathbf{A}_{\text{outer}}$, in which a complex network of $M \times N$ nodes arises.

The couplings are made bidirectionally, taking into account all state variables of each node, where each node constitutes an n -dimensional chaotic dynamical system, described as follows

$$\dot{\mathbf{x}}_i = \mathbf{f}(\mathbf{x}_i) + \mathbf{u}_i, \tag{1}$$

with $i = 1, 2, \dots, M \times N$, where $\mathbf{x}_i = (x_{i,1}, x_{i,2}, \dots, x_{i,n})^T \in \mathbb{R}^n$ is the state vector of node i , $\mathbf{u}_i = (u_{i,1}, u_{i,2}, \dots, u_{i,n})^T \in \mathbb{R}^n$ is the input signal of node i . In this work, an extensively studied and well-known diffusive coupling is used as follows:

$$\mathbf{u}_i = (\mathbf{A} \otimes \mathbf{\Gamma})\mathbf{x}_i, \tag{2}$$

where $\mathbf{\Gamma}_{n \times n}$ is an arbitrary diagonal matrix of zeros or ones, which involves the selection of state variables to be used in the inner and outer couplings, \otimes is the direct or Kronecker product, and $\mathbf{A}_{(M \times N) \times (M \times N)}$ is the total coupling matrix described as follows:

$$\mathbf{A} = c_1 \mathbf{A}_{\text{inner}} + c_2 \mathbf{A}_{\text{outer}} = c_1 (\mathbf{I} \otimes \mathbf{A}_i) + c_2 (\mathbf{A}_o \otimes \mathbf{\Gamma}_o), \tag{3}$$

where $\mathbf{A}_{\text{inner}(M \times N) \times (M \times N)}$ and $\mathbf{A}_{\text{outer}(M \times N) \times (M \times N)}$ are the inner and outer coupling matrices, c_1 and c_2 are the inner and outer coupling strengths, respectively, $\mathbf{I}_{M \times M}$ is the identity

matrix, $\Gamma_{o(N \times N)}$ is an arbitrary diagonal matrix of zeros or ones that involves the selection of nodes to be used in order to couple the networks, i.e., in the outer coupling, $A_{i(N \times N)}$ determines the inner topology, and $A_{o(M \times M)}$ determines the outer topology.

Now, suppose we have strongly connected complex networks (i.e., the complex networks are connected without isolated clusters). Then, A is a symmetric and irreducible matrix. In this case, it can be shown that zero is an eigenvalue of A with multiplicity 1 and all other eigenvalues are strictly negative, see [18,19]. Figures 1–3 show a graphic representation of the general scheme of the inner and outer coupling strategy to be used in this work, the left side of each figure shows the inner coupling topology to be used, while the right side shows the outer topology made up of the inner coupling topologies. According to [19], complex networks (1) achieve (asymptotic) synchronization, if

$$x_1(t) = x_2(t) = \dots = x_{M \times N}(t), \text{ as } t \rightarrow \infty. \tag{4}$$

It is desired that coupling conditions (2)–(3) guarantee that the synchronization state, $s(t) \in \mathbb{R}^n$, be a solution of an isolated node, which is

$$\dot{s}(t) = f(s(t)), \tag{5}$$

where $s(t)$ can be an equilibrium point, a periodic orbit, or a chaotic attractor. Thus, the stability of the synchronization state,

$$x_1(t) = x_2(t) = \dots = x_{M \times N}(t) = s(t), \tag{6}$$

of complex networks (1) is determined by the dynamics of the used chaotic system, described by the nonlinear function f and the solution $s(t)$, the coupling strengths c_1 and c_2 , the diagonal matrix Γ , and the coupling matrix A .

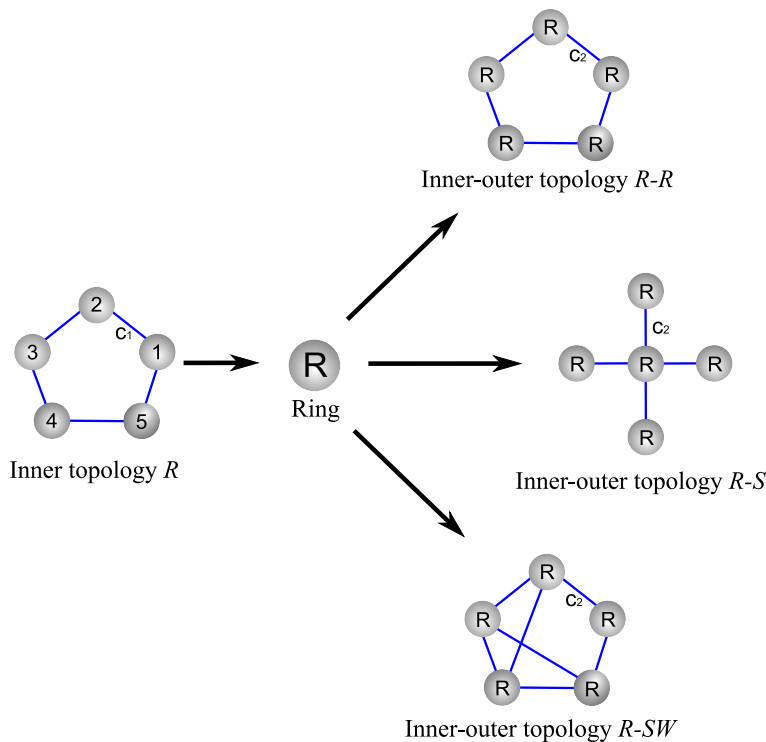


Figure 1. Inner-outer ring network coupling topology.

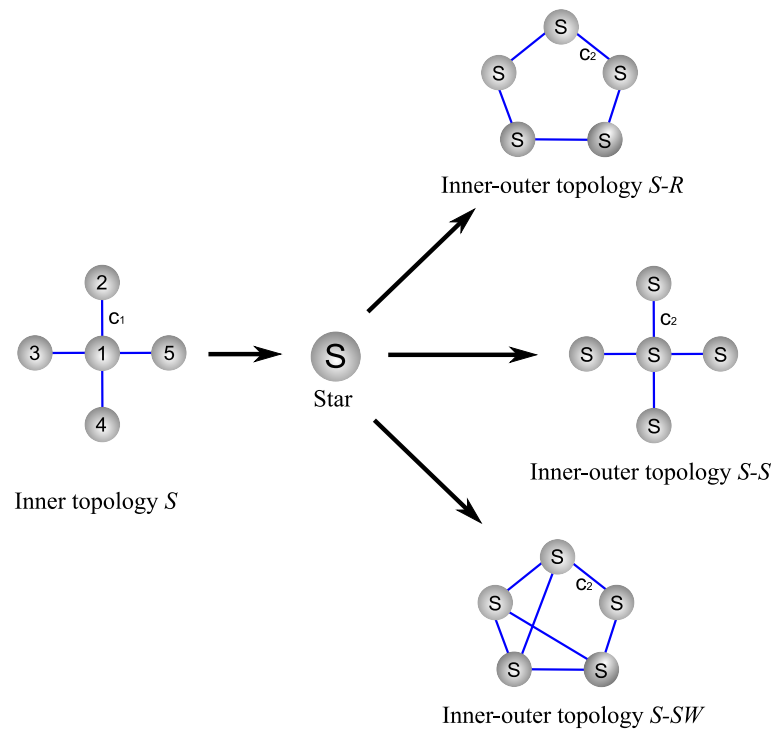


Figure 2. Inner-outer star network coupling topology.

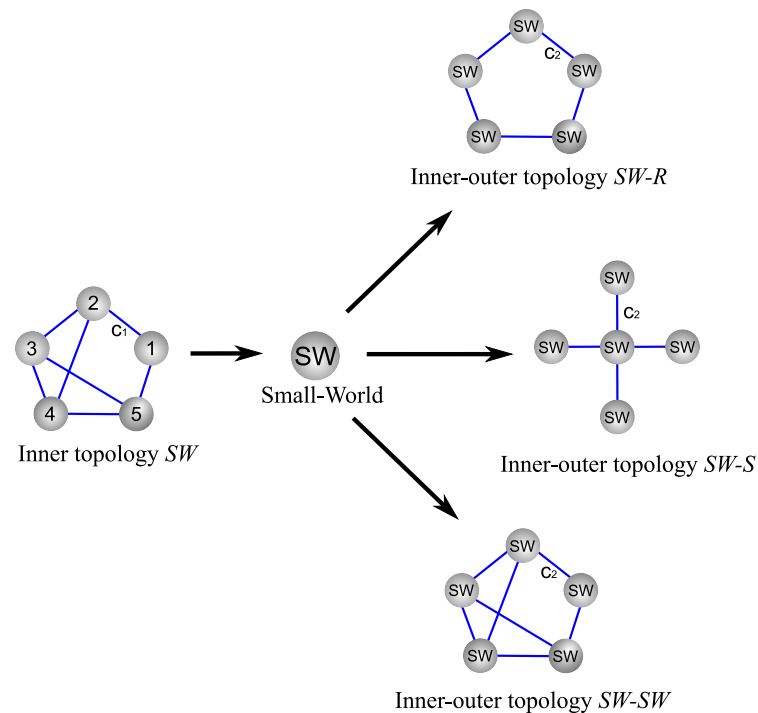


Figure 3. Inner-outer small-world network coupling topology.

3. Master Stability Function

This section describes the master stability function used to analyze the stability of the synchronization state on the inner-outer coupling topologies. In accordance with [20], and considering (2)–(3), each block of the diagonalized variational equation is described as follows:

$$\dot{\zeta}_k = [D\mathbf{f}(\mathbf{s}) + \zeta_k \mathbf{\Gamma}] \zeta_k, \tag{7}$$

with $k = 0, 1, 2, \dots, (M \times N) - 1$, where ζ_k is an eigenvalue of the coupling matrix \mathbf{A} , with $\zeta_0 = 0$. In this work, Γ is chosen, such that the coupling among the nodes of the networks is made using all of the state variables, so that, in this case, Γ is chosen as follows:

$$\Gamma = \begin{bmatrix} 1 & 0 & 0 \\ 0 & 1 & 0 \\ 0 & 0 & 1 \end{bmatrix}. \tag{8}$$

The maximum Lyapunov exponent λ_{max} is calculated for the generic variational Equation (7). By using certain inner and outer coupling strengths c_1 and c_2 , the sign of λ_{max} is verified, which indicates the synchronization state; for $\lambda_{max} < 0$, the synchronization state is stable, while for $\lambda_{max} > 0$, the synchronization state is unstable. For the computational calculation of the maximum Lyapunov exponents, we used a modified version of Wolf’s algorithm presented in [21]. To calculate the maximum Lyapunov exponents, we used the programming software Matlab with initial conditions $s(0) = [0, 0.1, 0]^T$ in the Ode45 function for a simulation time of 100 s.

4. Chaotic Node

In this section, we describe the chaotic system used, such as a chaotic node, in order to construct the inner–outer coupled networks. The chaotic system, which has hidden attractors and a coexistence property, is given by [22]:

$$\begin{bmatrix} \dot{x}_1 \\ \dot{x}_2 \\ \dot{x}_3 \end{bmatrix} = \begin{bmatrix} x_2 \\ -x_1 - x_2x_3 \\ |x_1| + x_1x_2 - a \end{bmatrix} \tag{9}$$

where $a \in \mathbb{R}^+$ and x_1, x_2, x_3 are state variables. Figure 4 shows the chaotic attractors in the phase planes x_1 vs. x_2 , x_1 vs. x_3 , and x_2 vs. x_3 of the system (9), which is obtained when $a = 1.35$, and the initial conditions are $(x_1, x_2, x_3) = (0, 0.1, 0)$.

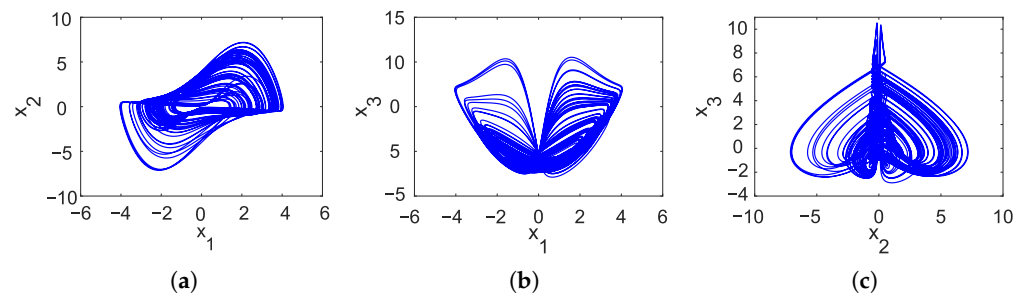


Figure 4. Phase planes of the chaotic system (9) with $a = 1.35$ (a) x_1 vs. x_2 phase plane; (b) x_1 vs. x_3 phase plane; (c) x_2 vs. x_3 phase plane.

There are coexisting attractors in system (9) when parameter $a = 1.4$. Figure 5 shows the hidden attractors in the phase planes x_1 vs. x_2 , x_1 vs. x_3 , and x_2 vs. x_3 for different initial conditions.

Due to the interesting dynamics that this system has when the value of the parameter a and its initial conditions are varied, the chaotic system was used as the chaotic node in order for the generated complex dynamics to be used in some applications, such as information encryption, see, for example, [23] and the generation of complex trajectories for tracking by mobile robots, see, for example, [24], among others.

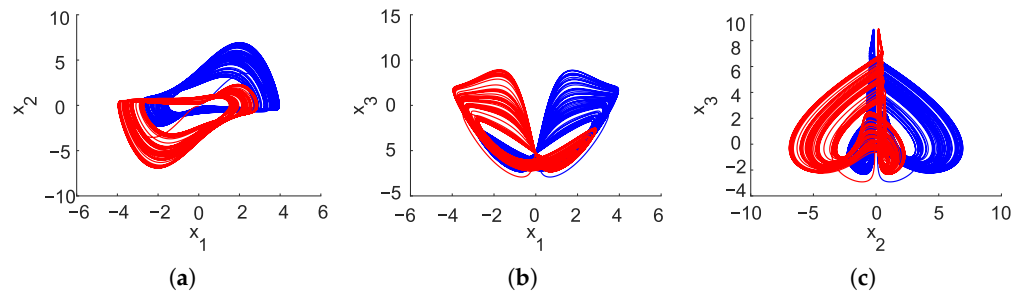


Figure 5. Phase planes of the chaotic system (9) with $a = 1.4$ and initial conditions $(x_1, x_2, x_3) = (0, 0.1, 0)$ (blue), and $(x_1, x_2, x_3) = (0, -0.1, 0)$ (red) (a) x_1 vs. x_2 phase plane; (b) x_1 vs. x_3 phase plane; (c) x_2 vs. x_3 phase plane.

5. Synchronization of Inner and Outer Coupling Topologies

This section analyzes and compares different inner–outer coupling network topologies. In the first instance, an analysis of the inner synchronizations of certain networks is presented, where synchronization states for different inner topologies are compared using the maximum Lyapunov exponent. On the other hand, the different connection topologies for the outer synchronizations of networks are also analyzed and compared, by means of the maximum Lyapunov exponent, considering a fixed value of c_1 , as well as through a comparison between c_1 vs. c_2 to determine which inner–outer coupling topology is the most optimal for outer synchronization among the networks. The representation of all nodes, for all of the above cases within the inner–outer coupling topologies, is as follows

$$\begin{bmatrix} \dot{x}_{i1} \\ \dot{x}_{i2} \\ \dot{x}_{i3} \end{bmatrix} = \begin{bmatrix} x_{i2} + u_{i1} \\ -x_{i1} - x_{i2}x_{i3} + u_{i2} \\ |x_{i1}| + x_{i1}x_{i2} - a + u_{i3} \end{bmatrix}, \tag{10}$$

where u_{i1} , u_{i2} , and u_{i3} are the control inputs using (2).

5.1. Inner Topologies of the Ring, Star, and Small-World Networks Synchronization

For the analysis of the ring, star, and small-world inner network topologies, first, we consider that each network is isolated from the other, i.e., if there is no outer synchronization of networks, then $c_2 = 0$ for a set of $M = 5$ networks composed of $N = 5$ nodes, where each node is a chaotic system, as described in (10) with exactly the same parameter values, as shown in Section 4. For the initial condition values, if node i is an even number, then we chose $\mathbf{x}_i(0) = [0 \quad -0.01i \quad 0]^T$; on the other hand, if node i is an odd number, then we chose $\mathbf{x}_i(0) = [0 \quad 0.01i \quad 0]^T$, with $i = 1, 2, \dots, N \times M$ nodes; the values of initial conditions are chosen in order to take advantage of the coexistence property possessed by the hidden attractor.

Now, in order to obtain the total coupling matrix \mathbf{A} , it is necessary to determine the coupling matrices $\mathbf{A}_{\text{inner}}$ and $\mathbf{A}_{\text{outer}}$, which determine the inner–outer coupling topologies. However, as seen in Equation (3), it is only necessary to obtain the Kronecker product between the topology matrix \mathbf{A}_i and the identity matrix $\mathbf{I}_{M \times M}$, since, as mentioned above, the inner synchronization of the networks is analyzed in isolation, i.e., $c_2 = 0$. Starting with the ring’s inner coupling network topology, the matrix is defined, such that

$$\mathbf{A}_i = \mathbf{A}_{i_{\text{ring}}} = \begin{bmatrix} -2 & 1 & 0 & 0 & 1 \\ 1 & -2 & 1 & 0 & 0 \\ 0 & 1 & -2 & 1 & 0 \\ 0 & 0 & 1 & -2 & 1 \\ 1 & 0 & 0 & 1 & -2 \end{bmatrix}, \tag{11}$$

for the star’s inner coupling network topology, the matrix A_i is defined as follows

$$A_i = A_{i_{star}} = \begin{bmatrix} -4 & 1 & 1 & 1 & 1 \\ 1 & -1 & 0 & 0 & 0 \\ 1 & 0 & -1 & 0 & 0 \\ 1 & 0 & 0 & -1 & 0 \\ 1 & 0 & 0 & 0 & -1 \end{bmatrix}, \tag{12}$$

Despite the regular topologies shown above, it should be noted that complex networks can be found everywhere and can be represented by random or regular topologies; however, a large number of real complex networks lies between these two extremes; that is, the topological structures are neither completely random nor regular. We could affirm that most of the technological, biological, and social networks are between these two extremes because these kinds of networks often have high clustering coefficients, such as regular networks, but with average path lengths similar to random networks, see [25]. These types of networks are called small-world networks, which are analogous to the small-world phenomenon (popularly known as the six degrees of separation).

In essence, these networks can be built from regular arrangements in which recon-nections are made or connections are added with a probability p to the chosen pairs of nodes. Even very small numbers of these added connections, commonly called shortcuts, do not change the local properties (such as very high clusterings, which are typical of regu-lar networks), but cause typical values of random networks in the average path lengths, see [26]. In this work, for the construction of small-world networks, we used the Newman and Watts model presented in [27], where we started with a ring-type coupling topology, then, using a probability $p_1 = 0.3$ of adding a connection between any pair of nodes, we obtained the small-world coupling matrix presented in (13) with a clustering coefficient of 0.4, an average path length of 1.04, and an average degree of 2.8. In this way, we define A_i for small-world inner coupling topology, as follows:

$$A_i = A_{i_{small}} = \begin{bmatrix} -2 & 1 & 0 & 0 & 1 \\ 1 & -3 & 1 & 1 & 0 \\ 0 & 1 & -3 & 1 & 1 \\ 0 & 1 & 1 & -3 & 1 \\ 1 & 0 & 1 & 1 & -3 \end{bmatrix}, \tag{13}$$

Now, we can calculate the maximum Lyapunov exponent λ_{max} of the variational Equation (7) for networks (10) built according to the coupling matrices (11)–(13) that define each inner coupling network topology. Figure 6 shows the maximum Lyapunov exponent λ_{max} against c_1 , where we can observe the inner coupling strength c_1 necessary to achieve inner synchronization in the R , S , and SW inner coupling network topologies.

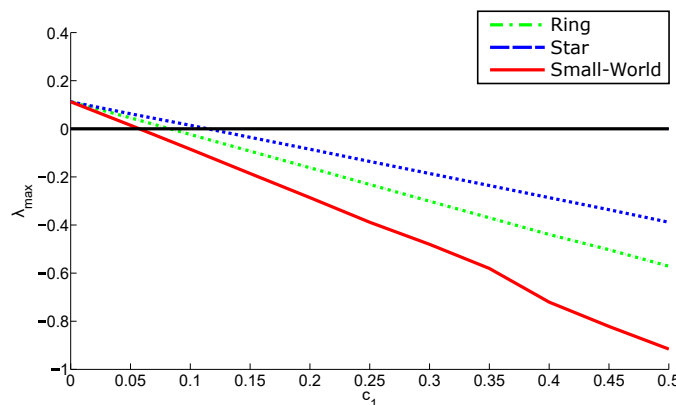


Figure 6. The maximum Lyapunov exponent λ_{max} with respect to c_1 for inner coupling network topologies R , S , and SW .

With the results shown in Figure 6, we can see that the best performance, in terms of minor coupling strength, is presented by the small-world network. On the other hand, to establish which inner–outer coupling network topology has the best performance, we present the corresponding analysis in the next subsection.

5.2. Outer Topology of Ring, Star, and Small-World Networks Synchronization

The main objective pursued in this work is to find a suitable coupling strength to achieve the outer synchronization of networks in different topologies, using chaotic systems with hidden attractors as nodes. This subsection presents a comparative analysis regarding outer synchronization and using different topologies according to the schemes shown in Figures 1–3, as well as their combinations. For this case, we use different combinations of inner and outer network topologies in order to perform a comparative analysis that allows us to reveal which of the combinations achieves an outer synchronization with a more suitable coupling strength. We use the notation presented in [28] to represent the different inner–outer coupling network topologies; for example, we use *R* for ring, *S* for star, and *SW* for small-world networks, i.e., for the inner ring and outer ring topologies, notation *R-R* is used (see Figure 1), for the inner star and outer star topologies, we use *S-S* (see Figure 2), for the inner small-world and outer small-world topologies, we use *SW-SW* (see Figure 3), and so on. Moreover, the constant diagonal matrix Γ_o that involves selecting nodes from the inner topologies for coupling with the outer topologies used in this work is described as follows:

$$\Gamma_o = \begin{bmatrix} 1 & 0 & 0 & 0 & 0 \\ 0 & 0 & 0 & 0 & 0 \\ 0 & 0 & 0 & 0 & 0 \\ 0 & 0 & 0 & 0 & 0 \\ 0 & 0 & 0 & 0 & 0 \end{bmatrix}. \tag{14}$$

If we take an inner–outer coupling topology *R-R* with $M = N = 5$, the matrix $\mathbf{A}_o = \mathbf{A}_{o_{ring}}$ is described as follows:

$$\mathbf{A}_{o_{ring}} = \mathbf{A}_{i_{ring}} = \begin{bmatrix} -2 & 1 & 0 & 0 & 1 \\ 1 & -2 & 1 & 0 & 0 \\ 0 & 1 & -2 & 1 & 0 \\ 0 & 0 & 1 & -2 & 1 \\ 1 & 0 & 0 & 1 & -2 \end{bmatrix}, \tag{15}$$

where $\mathbf{A}_{o_{ring}} \otimes \Gamma_o$ gives the matrix \mathbf{A}_{outer} . For inner–outer coupling topologies *S-S* and *SW-SW*, matrices $\mathbf{A}_o = \mathbf{A}_{o_{star}}$ and $\mathbf{A}_o = \mathbf{A}_{o_{sw}}$ are described as follows:

$$\mathbf{A}_{o_{star}} = \mathbf{A}_{i_{star}} = \begin{bmatrix} -4 & 1 & 1 & 1 & 1 \\ 1 & -1 & 0 & 0 & 0 \\ 1 & 0 & -1 & 0 & 0 \\ 1 & 0 & 0 & -1 & 0 \\ 1 & 0 & 0 & 0 & -1 \end{bmatrix}, \tag{16}$$

$$\mathbf{A}_{o_{sw}} = \mathbf{A}_{i_{sw}} = \begin{bmatrix} -2 & 1 & 0 & 0 & 1 \\ 1 & -3 & 1 & 1 & 0 \\ 0 & 1 & -3 & 1 & 1 \\ 0 & 1 & 1 & -3 & 1 \\ 1 & 0 & 1 & 1 & -3 \end{bmatrix}. \tag{17}$$

Consequently, Figure 7 shows the calculations of the maximum Lyapunov exponents λ_{max} for the inner–outer coupling network topologies *R-R*, *R-S*, *R-SW*, *S-R*, *S-S*, *S-SW*, *SW-R*, *SW-S*, and *SW-SW* for $c_1 = 0.5$ and $0 < c_2 < 2$.

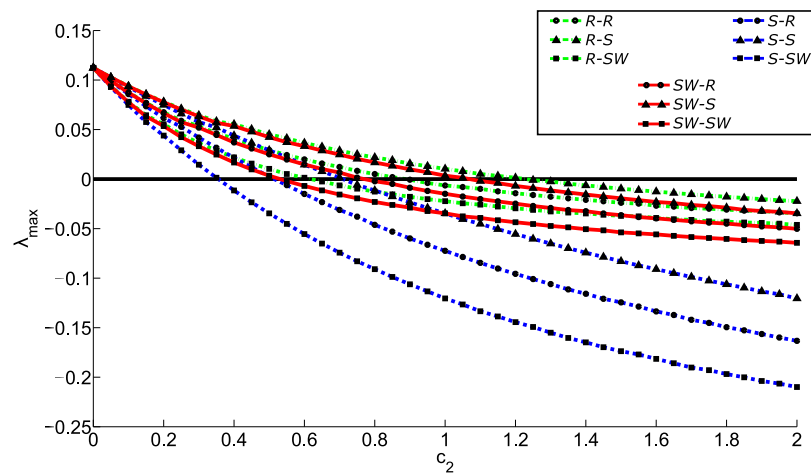


Figure 7. The maximum Lyapunov exponents λ_{max} for the inner–outer coupling topologies $R-R$, $R-S$, $R-SW$, $S-R$, $S-S$, $S-SW$, $SW-R$, $SW-S$, and $SW-SW$ for $c_1 = 0.5$ and $0 < c_2 < 2$.

Moreover, a comparison of the synchronization of the different inner–outer coupling network topologies is performed, where Figure 8 shows the maximum Lyapunov exponent λ_{max} for the inner–outer coupling topologies $R-R$, $R-S$, $R-SW$, $S-R$, $S-S$, $S-SW$, $SW-R$, $SW-S$, and $SW-SW$. In Figure 8, we can see the areas of synchronization and no synchronization for a sweep of c_1 versus c_2 with $0 \leq c_1, c_2 \leq 2$.

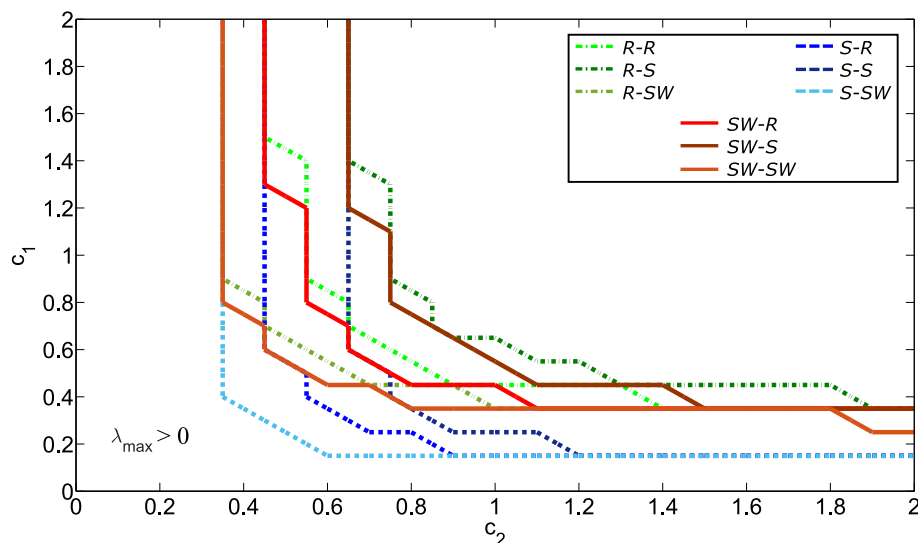


Figure 8. The maximum Lyapunov exponent λ_{max} for the inner–outer coupling topologies $R-R$, $R-S$, $R-SW$, $S-R$, $S-S$, $S-SW$, $SW-R$, $SW-S$, and $SW-SW$, considering a sweep of c_1 versus c_2 .

In order to corroborate the obtained results, temporal dynamics and synchronization errors for the most representative cases of inner–outer network coupling topologies are presented below. Figure 9 and 10 show the temporal dynamics and synchronization errors, respectively, for the case of the inner–outer network coupling topology $R-SW$, where we can see that for $0 < t < 20$ values of inner and outer coupling strengths $c_1 = 0$ and $c_2 = 0$ are applied, indicating that all nodes are uncoupled; for $20 \leq t < 60$, the inner and outer coupling strength values $c_1 = 0.5$ and $c_2 = 0$ are applied, meaning that the networks are coupled internally but uncoupled externally; for $t \geq 60$, the inner and outer coupling strength values $c_1 = 0.5$ and $c_2 = 0.4$ are applied, indicating that there is inner and outer coupling among the networks. For coupling strength values $c_1 = 0.5$ and $c_2 = 0.4$, we can see that synchronization is achieved both internally and externally, corroborating the findings presented in Figure 8.

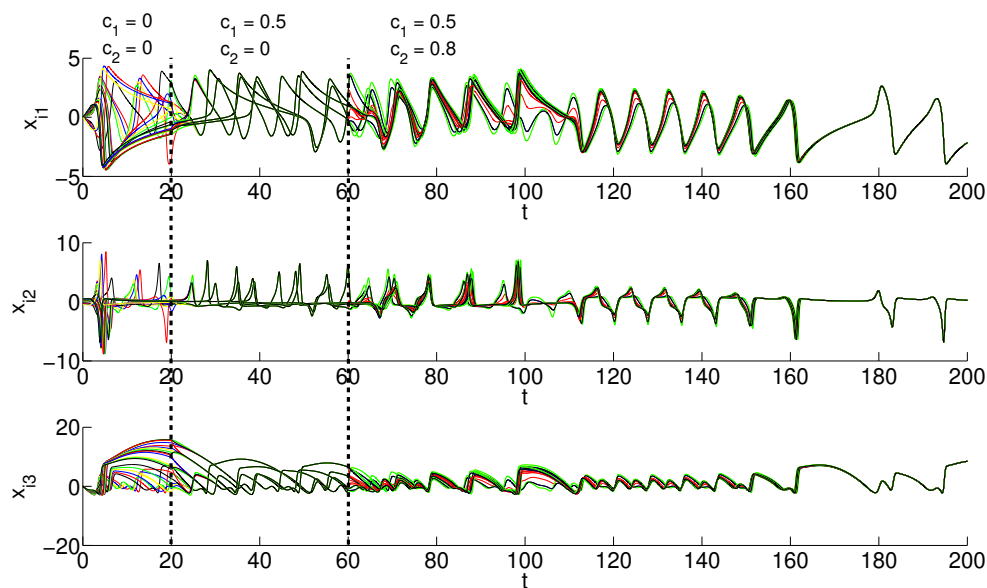


Figure 9. Temporal dynamics of the inner–outer network coupling topology *R-SW* for different values of c_1 and c_2 , where the colors are to differentiate the states of each node.

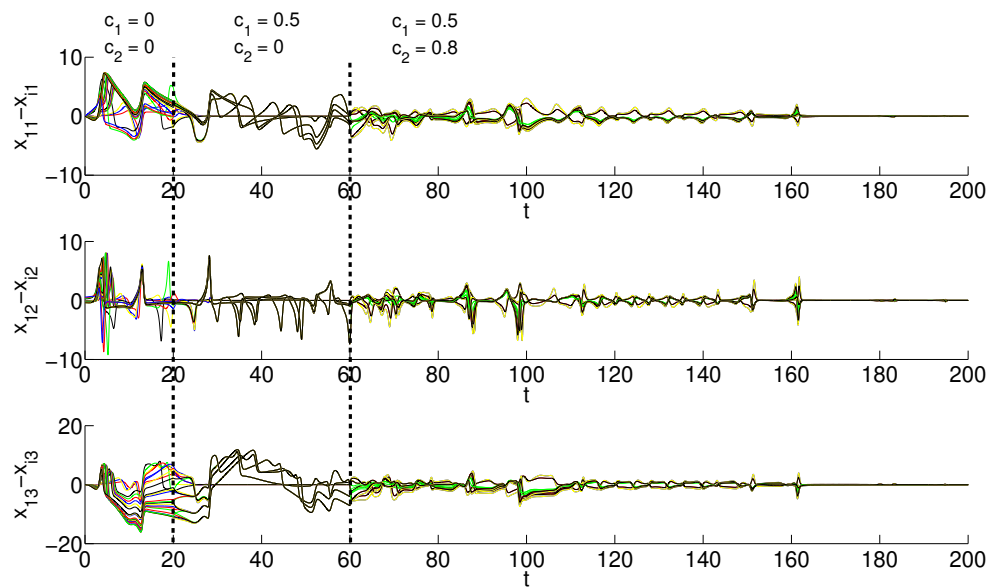


Figure 10. Synchronization error of the inner–outer network coupling topology *R-SW* for different values of c_1 and c_2 , where the colors are to differentiate the states of each node.

We proceed in the same way for the cases of inner–outer network coupling topologies *S-SW* and *SW-SW*, where Figures 11–14 show the temporal dynamics and synchronization errors of topologies *S-SW* and *SW-SW*, respectively.

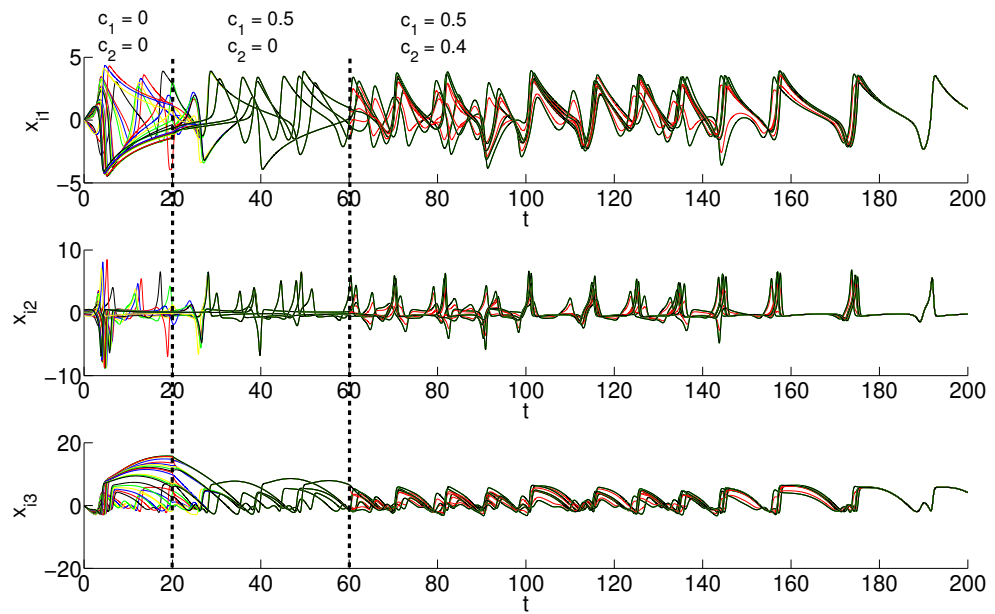


Figure 11. Temporal dynamics of the inner–outer network coupling topology *S-SW* for different values of c_1 and c_2 , where the colors are to differentiate the states of each node.

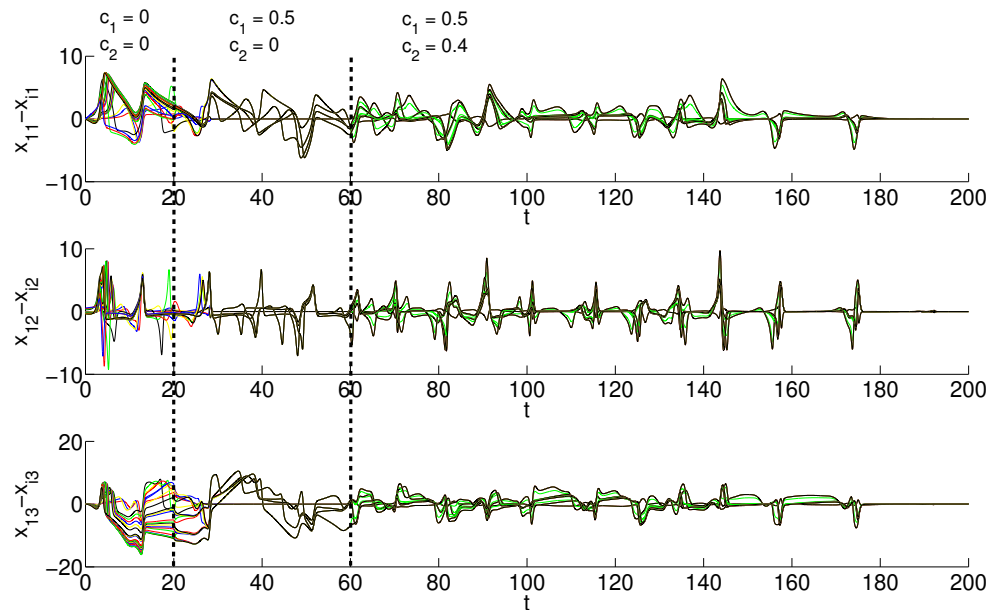


Figure 12. Synchronization error of the inner–outer network coupling topology *S-SW* for different values of c_1 and c_2 , where the colors are to differentiate the states of each node..

As we can see, the obtained results regarding temporal dynamics and the synchronization errors are in accordance with what is presented in Figure 8, where we can establish that *S-SW* is the most suitable inner–outer bidirectional coupling network topology to achieve outer synchronization. To complement the study using $M = N = 5$, we consider increasing N and M , taking into account the number of nodes of an example of a small-world network presented in [27], where, for this case, we have $M = N = 24$. To build the small-world network, in the same way as in the case with $N = 5$, we choose $p_1 = 0.3$, although it is true that the average of a certain number of generated small-world networks must be analyzed and the effects caused would have to be considered, this has been left as an open problem for future work. In this case, for the fixed topology of the small-world network, the numerical representation is omitted due to the large dimensions of the generated coupling network topology, where a clustering coefficient of 0.5388, an average path length of 1.3924,

and an average degree of 12.5833 are obtained. Figure 15 shows the maximum Lyapunov exponent λ_{max} in a similar way as in Figure 8, where, for this case, due to the ranges of the separation of the coupling strengths c_1 and c_2 , only the comparisons of inner–outer coupling topologies S-SW and S-SW are shown, since it has been verified that S-SW and S-SW overlap the other inner–outer coupling topologies R-R , R-S, R-SW, S-R, S-S, SW-R, and SW-S. Note that, from Figure 15, it is shown that the results for $N = 5$ and $M = 5$ can be extended to a greater number of nodes N and networks M , preserving the obtained results for $N = M = 5$, where the best performance to achieving outer synchronization is by using the S-SW inner–outer coupling network topology.

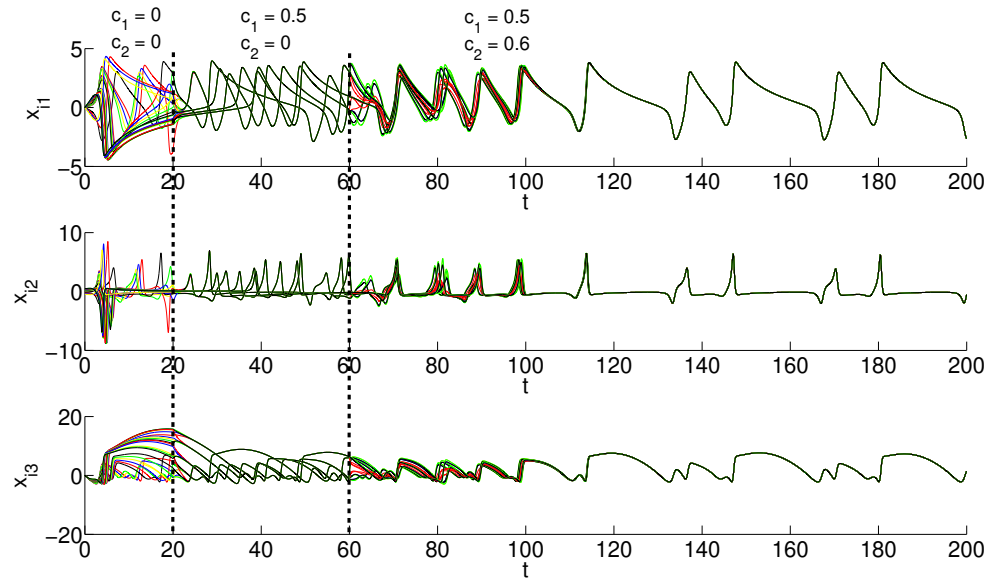


Figure 13. Temporal dynamics of the inner–outer network coupling topology SW-SW for different values of c_1 and c_2 , where the colors are to differentiate the states of each node.

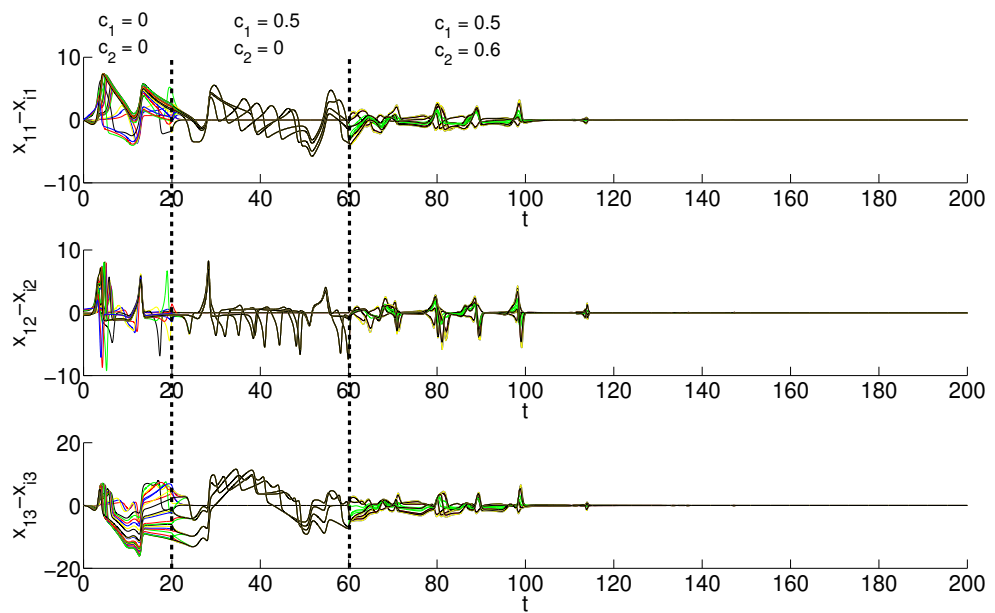


Figure 14. Synchronization error of the inner–outer network coupling topology SW-SW for different values of c_1 and c_2 , where the colors are to differentiate the states of each node.

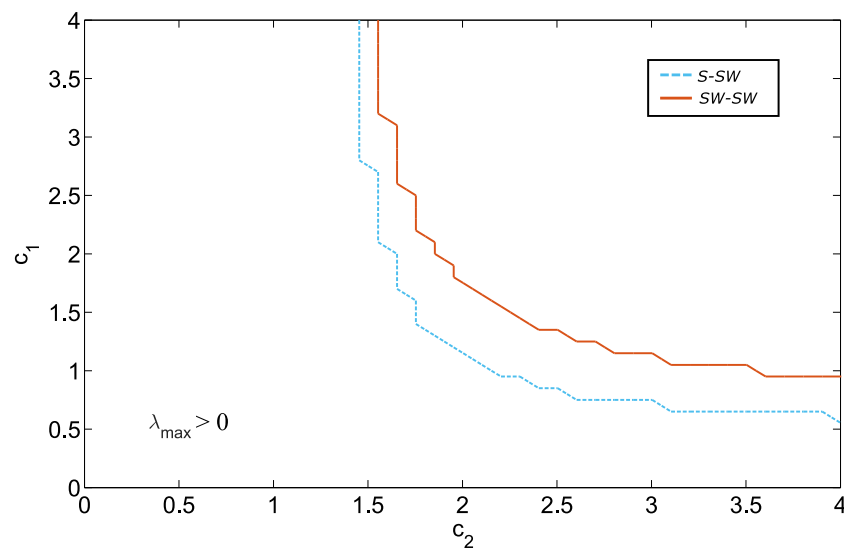


Figure 15. The maximum Lyapunov exponent λ_{max} for the inner–outer coupling topologies S-SW, and SW-SW for $N = M = 24$.

6. Conclusions

From this work, which is based on the use of a master stability function approach (the maximum Lyapunov exponent λ_{max} of the generic variational equations) to determine the suitable inner and outer coupling strengths to achieve synchronization, we established that the most suitable bidirectional inner–outer coupling topology combination to achieve outer synchronization is the S-SW topology. Additionally, the obtained results (by means of the master stability function approach) were corroborated through the numerical calculation of the temporal dynamics and synchronization errors of some particular and representative cases. Furthermore, it is possible to obtain complementary results to this study by using a different number of nodes N or a different number of networks M . It is also possible to use different discrete or continuous chaotic nodes of different dimensions or fractional orders, conduct a number of realizations of the small-world network model, study the average behavior, etc. Moreover, the obtained results can be used in potential applications, such as the synchronization of mobile robots, sending messages safely, and in electric power distribution networks, among others.

Author Contributions: Conceptualization, C.A.V.-A., A.A.-D., E.Z.-S., J.P.-J. and C.C.-H.; methodology, C.A.V.-A., A.A.-D., E.Z.-S., J.P.-J. and C.C.-H.; software, C.A.V.-A., A.A.-D., E.Z.-S., J.P.-J. and C.C.-H.; validation, C.A.V.-A., A.A.-D., E.Z.-S., J.P.-J. and C.C.-H.; formal analysis, C.A.V.-A., A.A.-D., E.Z.-S., J.P.-J. and C.C.-H.; investigation, C.A.V.-A., A.A.-D., E.Z.-S., J.P.-J. and C.C.-H.; writing—original draft preparation, C.A.V.-A., A.A.-D., E.Z.-S., J.P.-J. and C.C.-H.; writing—review and editing, C.A.V.-A., A.A.-D., E.Z.-S., J.P.-J. and C.C.-H.; visualization, C.A.V.-A., A.A.-D., E.Z.-S., J.P.-J. and C.C.-H. All authors have read and agreed to the published version of the manuscript.

Funding: This research was funded by Consejo Nacional de Ciencia y Tecnología (166654 (A1-S-31628)) and CF-2023-I-1110.

Institutional Review Board Statement: Not applicable.

Data Availability Statement: The data used to support the findings of this study are included within the article.

Acknowledgments: A.A.-D. is a CONACYT research fellow commissioned to the Universidad Autónoma de Baja California (Project no. 3059). J.P.-J. is a CONACYT research fellow commissioned to the Scientific Research and Advanced Studies Center of Ensenada (Project no. 1030). E.Z.-S., acknowledges CONACYT-Mexico Research grant no. CF-2023-I-1110, and “Departamento de Electrónica y Automatización” from Facultad de Ingeniería Mecánica y Eléctrica at UANL.

Conflicts of Interest: The authors declare no conflict of interest.

References

1. Pikovsky, A.; Rosenblum, M.; Kurths, J. A universal concept in nonlinear sciences. *Self* **2001**, *2*, 3.
2. Blasius, B.; Huppert, A.; Stone, L. Complex dynamics and phase synchronization in spatially extended ecological systems. *Nature* **1999**, *399*, 354–359. [[CrossRef](#)] [[PubMed](#)]
3. Watts, D.J.; Strogatz, S.H. Collective dynamics of ‘small-world’ networks. *Nature* **1999**, *393*, 440–442. [[CrossRef](#)] [[PubMed](#)]
4. Zambrano-Serrano, E.; Muñoz-Pacheco, J.M.; Anzo-Hernández, A.; Félix-Beltrán, O.G.; Guevara-Flores, D.K. Synchronization of a cluster of β -cells based on a small-world network and its electronic experimental verification. *Eur. Phys. J. Spec. Top.* **2022**, *231*, 1035–1047. [[CrossRef](#)]
5. Arellano-Delgado, A.; López Gutiérrez, R.M.; Cruz-Hernández, C.; Martínez-Clark, R. Small-World Outer Synchronization of Small-World Chaotic Networks. *J. Comput. Nonlinear Dyn.* **2018**, *13*, 101008. [[CrossRef](#)]
6. Arellano-Delgado, A.; López Gutiérrez, R.M.; Méndez-Ramírez, R.; Cardoza-Avenidaño, L.; Cruz-Hernández, C. Dynamic coupling in small-world outer synchronization of chaotic networks. *Phys. D Nonlinear Phenom.* **2021**, *423*, 132928. [[CrossRef](#)]
7. Sun, J.; Bollt, E.M.; Porter, M.A.; Dawkins, M.S. A mathematical model for the dynamics and synchronization of cows. *Phys. D* **2011**, *240*, 1497–1509. [[CrossRef](#)]
8. Bowen, T.A.; Zhivun, E.; Wickenbrock, A.; Dumont, V.; Bale, S.D.; Pankow, C.; Dobler, G.; Wurtele, J.S.; Budker, D. A network of magnetometers for multi-scale urban science and informatics. *Geosci. Instrum. Methods Data Syst.* **2019**, *8*, 129–138. [[CrossRef](#)]
9. Arenas, A.; Díaz-Guilera, A.; Kurths, J.; Moreno, Y.; Zhou, C. Synchronization in complex networks. *Phys. Rep.* **2008**, *469*, 93–153. [[CrossRef](#)]
10. Zou, C.; Wei, X.; Zhang, Q.; Liu, Y. Synchronization of chemical reaction networks based on DNA strand displacement circuits. *IEEE Access* **2018**, *6*, 20584–20595. [[CrossRef](#)]
11. Lü, L.; Zhang, F.; Zou, C. Finite-time synchronization in the laser network based on sliding mode control technology. *Optik* **2021**, *225*, 165605. [[CrossRef](#)]
12. Lü, L.; Zhao, L. Finite-time synchronisation transmission of quantum signals between Jaynes-Cummings models based on coupling technology. *Opt. Quantum Electron.* **2023**, *55*, 145. [[CrossRef](#)]
13. López-Mancilla, D.; López-Cahuich, G.; Posadas-Castillo, C.; Castañeda, C.E.; García-López, J.H.; Vázquez-Gutiérrez, J.L.; Tlelo-Cuautle, E. Synchronization of complex networks of identical and nonidentical chaotic systems via model-matching control. *PLoS ONE* **2019**, *14*, e0216349. [[CrossRef](#)]
14. Strogatz, S.H. *Sync: How Order Emerges from Chaos in the Universe, Nature, and Daily Life*, 1st ed.; Westport, CO, USA, 2003.
15. Sun, W.; Yan, Z.Z.; Chen, S.H.; Lü, J.H. Outer synchronization of complex networks by impulse. *Commun. Theor. Phys.* **2011**, *56*, 885. [[CrossRef](#)]
16. Wang, L.; Zhang, J.; Sun, W. Adaptive outer synchronization and topology identification between two complex dynamical networks with time-varying delay and disturbance. *IMA J. Math. Control. Inf.* **2019**, *36*, 949–961. [[CrossRef](#)]
17. Kuznetsov, N.V. Theory of Hidden Oscillations and Stability of Control Systems. *J. Comput. Syst. Sci. Int.* **2020**, *59*, 647–668. [[CrossRef](#)]
18. Wang, X.F.; Chen, G. Synchronization in small-world dynamical networks. *Int. J. Bifurc. Chaos* **2002**, *12*, 187–192. [[CrossRef](#)]
19. Wang, X.F. Complex networks: Topology, dynamics and synchronization. *Int. J. Bifurc. Chaos* **2002**, *12*, 885–916. [[CrossRef](#)]
20. Pecora, L.M.; Carroll, T.L. Master Stability Functions for Synchronized Coupled Systems. *Phys. Rev. Lett.* **1997**, *80*, 2109–2112. [[CrossRef](#)]
21. Wolf, A.; Swift, J.B.; Swinney, H.L.; Vastano, J.A. Determining Lyapunov exponents from a time series. *Phys. D Nonlinear Phenom.* **1985**, *16*, 285–317. [[CrossRef](#)]
22. Pham, V.T.; Volos, C.; Jafari, S.; Kapitaniak, T. Coexistence of hidden chaotic attractors in a novel no-equilibrium system. *Nonlinear Dyn.* **2017**, *87*, 2001–2010. [[CrossRef](#)]
23. Reyes-De la Cruz, D.; Méndez-Ramírez, R.; Arellano-Delgado, A.; Cruz-Hernández, C. Electronic Implementation of a Deterministic Small-World Network: Synchronization and Communication. *Entropy* **2023**, *25*, 709. [[CrossRef](#)] [[PubMed](#)]
24. Cetina-Denis, J.J.; López-Gutiérrez, R.M.; Cruz-Hernández, C.; Arellano-Delgado, A. Design of a Chaotic Trajectory Generator Algorithm for Mobile Robots. *Appl. Sci.* **2022**, *12*, 2587. [[CrossRef](#)]
25. Newman, M.E.J.; Barabási, A.-L. *The Structure and Dynamics of Networks*; Princeton University Press: Princeton, NJ, USA, 2006.
26. Dorogovtsev, S.N.; Mendes, J.F.; Dorogovtsev, S.N. *Evolution of Networks: From Biological Nets to the Internet and WWW*; Oxford University Press: Oxford, UK, 2003.
27. Newman, M.E.J.; Watts, D.J. Scaling and percolation in the small-world network model. *Phys. Rev. E* **1999**, *60*, 7332–7342. [[CrossRef](#)]
28. Arellano-Delgado, A.; López-Gutiérrez, R.M.; Murillo-Escobar, M.A.; Posadas-Castillo, C. Master—Slave Outer Synchronization in Different Inner—Outer Coupling Network Topologies. *Entropy* **2023**, *25*, 707. [[CrossRef](#)]

Disclaimer/Publisher’s Note: The statements, opinions and data contained in all publications are solely those of the individual author(s) and contributor(s) and not of MDPI and/or the editor(s). MDPI and/or the editor(s) disclaim responsibility for any injury to people or property resulting from any ideas, methods, instructions or products referred to in the content.